

Structural and electronic properties of V_2O_5 and their tuning by doping with 3d elements – Modelling with DFT+ U method and dispersion correction

A. Jovanović^{1,2}, A. S. Dobrota¹, L. D. Rafailović², S. V. Mentus^{1,3}, I. A. Pašti^{1,4*}, B. Johansson^{4,5}, N. V. Skorodumova^{4,5}

¹*University of Belgrade - Faculty of Physical Chemistry, Belgrade, Serbia*

²*CEST Center of Electrochemical Surface Technology, Wiener Neustadt, Austria*

³*Serbian Academy of Sciences and Arts, Belgrade, Serbia*

⁴*Department of Materials Science and Engineering, KTH - Royal Institute of Technology, Stockholm, Sweden*

⁵*Department of Physics and Astronomy, Uppsala University, Uppsala, Sweden*

Abstract

New electrode materials for alkaline-ion batteries are a timely topic. Among many promising candidates, V_2O_5 is one of the most interesting cathode materials. While having very high theoretical capacity, in practice, its performance is hindered by low stability and poor conductivity. As regards theoretical descriptions of V_2O_5 , common DFT-GGA calculations fail to reproduce both the electronic and crystal structure. While the band gap is underestimated, the interlayer spacing is overestimated as weak dispersion interactions are not properly described within GGA. Here we show that the combination of the DFT+ U method and semi-empirical D2 correction can compensate for the drawbacks of the GGA approximation when it comes to the modelling of V_2O_5 . When compared to common PBE calculations, with a modest increase of the computational cost, PBE+ U +D2 fully reproduced the experimental band gap of V_2O_5 , while the errors in the lattice parameters are only a few percent. Using the proposed PBE+ U +D2 methodology we studied V_2O_5 doped with 3d elements (from Sc to Zn). We show that both the structural and electronic parameters are affected by doping. Most importantly, a significant increase of conductivity is expected upon doping, which is of great importance for the application of V_2O_5 in metal-ion batteries.

Keywords: vanadium pentoxide; structure and electronic properties; doping; theoretical modelling

* Corresponding author, e-mail: igor@ffh.bg.ac.rs

1. Introduction

Alkaline metal-ion batteries are ones of the most commonly used and investigated electrochemical power sources of today. Among these, Li-ion batteries (LIBs) provide the highest energy density and the best cycle life. Although they show an appreciable performance, the search for new electrode materials for these systems continues [1,2]. Widely used electrodes, like LiMn_2O_4 , LiCoO_2 , and LiNiO_2 , provide a noticeable performance and have found their application in commercial devices in spite of some drawbacks. Namely, the first commercial cathode material, LiCoO_2 , although having a high theoretical capacity, can effectively deliver only around 150 mA h g^{-1} , in addition to its high price and pronounced toxicity [3]. In contrast to the mentioned materials, vanadium pentoxide (V_2O_5) attracted significant attention of the research community due to its high energy density, low cost, easy preparation, availability, and relatively safe use [4–7]. With the theoretical capacity of approx. 294 mA h g^{-1} V_2O_5 outperforms commonly used cathode materials, making it a very promising cathode material for the next-generation of LIBs. In fact, the interest in V_2O_5 as an electrode material for rechargeable batteries (LIBs and other types of metal-ion batteries) has been revitalized due to the use of lithium metal as anode [3] and extensive search for cathode materials beyond LIBs [3,8–11]. The layered structure of V_2O_5 allows metal ion intercalation in-between V_2O_5 layers, causing the texture and morphology changes when metal ions are introduced into the structure [12]. While the electrode materials obtained from V_2O_5 show higher energy and power density, and are generally easier to prepare than conventional materials, the main drawback is the decrease in capacity during cycling, which is assumed to arise from the issues associated with low conductivity and material degradation [13].

One of the strategies to overcome the problems related to stability and to improve the electrode performance of V_2O_5 is doping by various transition metals [14,15]. There are numerous reports in the literature showing the improved performance of doped V_2O_5 materials in rechargeable metal-ion batteries. As good examples, one can mention reports regarding the increased electronic conductivity of amorphous V_2O_5 upon doping with Ag, Cu, and Zn [16–21]. Also, an improved electrode performance was reported upon V_2O_5 doping with Mn [22]. In addition, versatile nanostructures of Cu-doped V_2O_5 [23,24], Fe-doped V_2O_5 [25] and Cr-doped V_2O_5 [26] were reported as cathodes for rechargeable metal-ion batteries, all witnessing an improved stability and better intercalation behavior of metal ions compared to pure V_2O_5 .

Besides the large body of experimental work, V_2O_5 was also investigated theoretically, but to a lower extent. V_2O_5 is rather challenging for conventional Density Functional Theory (DFT), since due to correlation effects DFT methods underestimate the band gap and cannot

account for dispersion interactions important for the description of V_2O_5 [27]. In order to overcome the first problem, DFT+ U approach [28,29] is often applied with satisfactory results [30,31]. The problem of the crystal structure description is addressed either by addition of (semi) empirical vdW-terms to the GGA calculations [32] or using vdW-DF methods [33]. In particular Londero and Schröder [33,34] have shown that GGA-PBE and GGA-PW91 approaches, either using ultrasoft pseudopotentials or PAW approach, significantly overestimate the interlayer spacing (around ~12%). The same authors have shown that the predicted structure is also very sensitive to the choice of the exchange-correlation functional within vdW-DF1 [35,36] and vdW-DF2 methods [37]. In fact, some of these functionals perform almost as poor as GGA-PBE in terms of structure description, while the energies of the interactions between V_2O_5 layers are estimated better. However, within the later approach the electronic structure of V_2O_5 is not described properly. To make the situation even more confusing, there are reports showing rather good agreement between the GGA results (PW91 results [30]) and experimental crystal structure. However, the agreement between theory and experiment became worse upon the addition of the on-site Coulomb correlation for the V $3d$ orbitals, in the attempt to describe the electronic structure better [30].

As an adequate description of both electronic and crystal structures is required for a better understanding of materials performance, here we present a systematic analysis of V_2O_5 using plane wave DFT calculations. We show that a proper description of this material can be obtained by combining the DFT+ U approach with the semi-empirical correction for the long range dispersion in the DFT+D2 formulation of Grimme [38]. We further use this approach to investigate the properties of V_2O_5 doped with $3d$ transition metals and discuss the obtained results in terms of possible energy storage application of doped V_2O_5 .

2. Computational details

The DFT calculations were performed using the GGA approximation within Perdew–Burke–Ernzerhof parametrization for the exchange correlation functional [39], applying the Quantum ESPRESSO (QE) *ab initio* package [40]. The pseudopotential method with ultrasoft pseudopotentials (USPP) [41], as implemented in QE, was used. The kinetic energy cutoff for the plane-wave basis set was 35 Ry, while the charge density cutoff was 16 times higher. Spin polarization was included in all the calculations. A simplified version of DFT+ U developed by Cococcioni and de Gironcoli [42] was used. The on-site Coulomb interaction was considered only for the vanadium $3d$ states and the value of U was changed systematically between 2 eV and 6 eV. In order to account for the long range dispersion interactions the semi-empirical

correction in the formulation of Grimme (DFT+D2) was applied [38]. The Brillouin zone was sampled using a Γ -centered k-point mesh, while a small Gaussian smearing was applied to improve the convergence.

We doped V_2O_5 by 3d transition metals (denoted hereafter as M) both interstitially, between the layers of V_2O_5 , and substitutionally, by replacing one of the V atoms in the simulation cell. The simulation cell was constructed as a (1x1x2) supercell of V_2O_5 , containing two V_2O_5 layers along the z-direction of the cell. The doping was done in every second layer or in-between layers, resulting in the stoichiometry corresponding to $M_{0.25}V_{1.75}O_5$ (substitutional doping) or $M_{0.25}V_2O_5$ (interstitial doping). The concentration of dopants is somewhat larger than the ones usually considered experimentally, although in some cases even higher concentrations of dopants were used. Nevertheless, we are interested in the overall trends and consider them to be accounted properly using the same concentration of dopants for all systems. As will be discussed later on, for doped V_2O_5 we applied U to the V 3d states only. Variable cell dynamics was used for structural optimization allowing both the cell and atomic positions to relax. Following the optimization, all the structures were recalculated in order to account for the change in basis set. Graphics presented in this work was made using either the VMD code [43] or VESTA [44].

3. Results and discussion

3.1. Pristine V_2O_5

We first discuss the crystal structure of pristine V_2O_5 and the impact of the applied computational scheme on the obtained crystal structure parameters (Fig. 1). A clear trend in the calculated lattice parameters *versus* increasing U is seen: parameter a decreases, while parameters b and c increase. While the relative errors obtained for a and b are less than 3% with respect to the experimental values, that is typical for PBE, parameter c , corresponding to the interlayer spacing, is overestimated by more than 13% and the error increases with the value of U (Fig. 1). Similar relative errors for parameter c (11.2%) were previously reported by Kerber *et al.* [32], who applied PBE combined with the PAW approach. The same authors were able to reduce the error down to 2.97% by adding the correction for dispersion interactions (with a and b fixed to the experimental values). Similarly, Londero and Schröder [34] reported parameter c , which was overestimated by 11.5% and 12% for PBE with PAW and USPP, respectively. The work of Ganduglia-Pirovano and Sauer [45], using PW91 functional combined with PAW approach, overestimates c by 10.8%. All these results reflect a well-accepted fact that the interlayer interactions in bulk V_2O_5 are very weak and dispersive in nature.

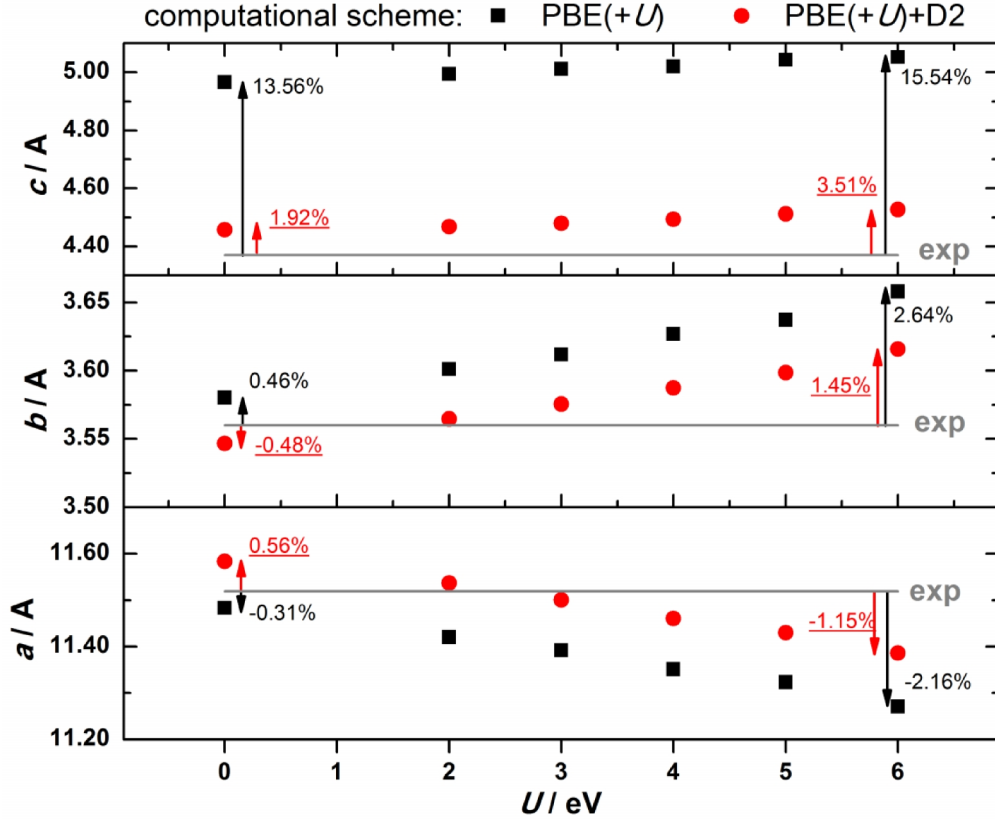


Figure 1. Dependence of the unit cell parameters of pristine V_2O_5 on the applied value of U , depending whether DFT+D2 correction was applied (circles) or no (squares). $U = 0$ is equivalent to plain PBE or PBE+D2. Indicated numbers give the relative errors (in %) of calculated lattice parameters with respect to the experimental values (underlined numbers are for PBE+ U +D2 scheme).

Whereas the addition of on-site Coulombic U applied to the vanadium d -states further increases the parameter c , the addition of the dispersion term compensates for this effect (Fig. 1). When PBE+D2 is applied, the error for c is reduced down to 1.92%, i.e. 7 times compared to the PBE result. The impact of U on the lattice parameters is noticeable and it remains the same irrespectively on the addition of D2 correction. Therefore, we conclude that the addition of the D2 correction to PBE+ U allows for the estimation of the lattice parameters with the relative error of a few percent only. Errors in the calculated lattice parameters are also translated into an overestimated unit cell volume (Fig. 2). It is clearly seen that the unit cell volume increases with U , with a relative error between 14% and 16% when dispersion interactions between the V_2O_5 layers are disregarded. This error arises almost exclusively from the error in parameter c and it is efficiently removed upon the addition of D2 correction. Even for the highest value of U the relative error found for the unit cell volume is below 4%, which we consider as an important

improvement. When it comes to the battery applications of V_2O_5 , the interlayer space provides the important diffusion paths for metal ions. Therefore, an incorrect interlayer distance would result in erroneous estimates of ion mobility in V_2O_5 .

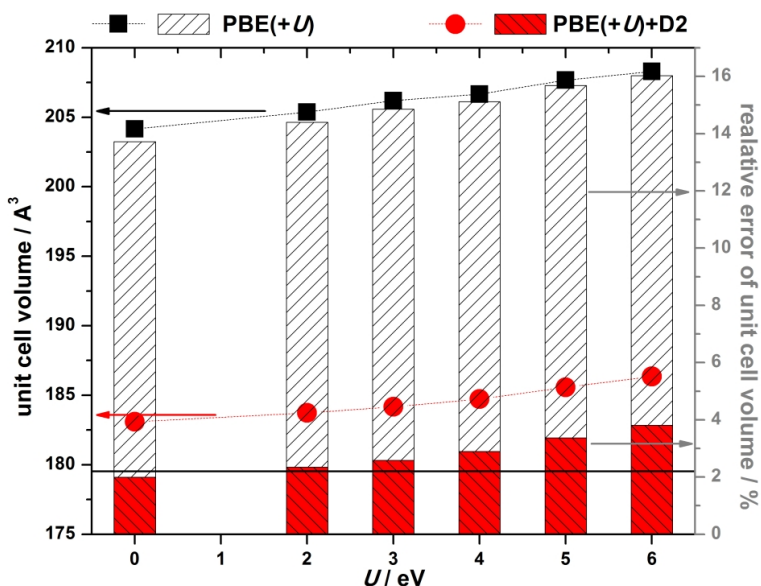


Figure 2. Unit cell volume of pristine bulk V_2O_5 depending on the value of U for PBE+ U (squares) and PBE+ U +D2 (circles). Relative errors are given by vertical bars. Experimental value of the unit cell volume (179.53 \AA^3) is given by thick horizontal line. When $U = 0 \text{ eV}$, calculations are performed at PBE(+D2) level.

Let us now look at how well the electronic structure is described within the PBE+ U +D2 approach. Fig. 3 shows that the band gap, width increases practically linearly with U , from $\sim 1.6 \text{ eV}$ (PBE and PBE+D2, $U = 0 \text{ eV}$) to $\sim 2.3 \text{ eV}$ (PBE+ U and PBE+ U +D2, $U = 6 \text{ eV}$). The width of the valence band (around 5.5 eV) depends weakly on U and agrees with previously reported values [30,46]. The band gap is correctly estimated for higher values of U ($U = 5 \text{ eV}$ and $U = 6 \text{ eV}$). The experimentally determined values of the band gap of V_2O_5 are 2.0 eV [47] and 2.2 eV [48], while Meyer *et al.* [49] have recently reported a bit larger value of 2.8 eV using the combination of ultraviolet, inverse and x-ray photoemission spectroscopy.

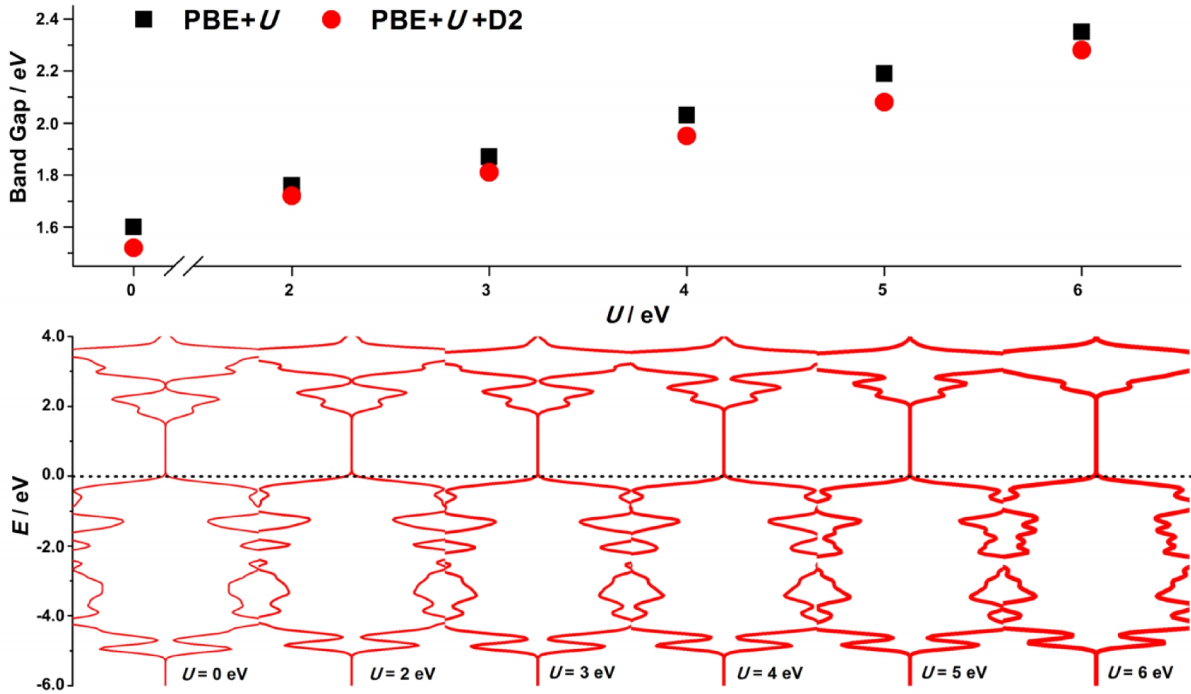


Figure 3. Calculated band gaps of pristine bulk V_2O_5 using PBE+ U (squares) and PBE+ U +D2 (circles), top, and density of states (DOS) obtained using PBE+ U +D2 approach. Top of the valence band is set to 0 eV.

The band gap determined with PBE is 1.6 eV, in agreement with previous work where the same level of theory has been used [30,50]. The gap calculated with PBE+ U shows better agreement with the experimental result, but it depends on the value of U and the applied DFT+ U scheme. Most frequently, the approach of Dudarev *et al.* [29] is applied with U_{eff} equal 3 eV or higher. Although the gap values close to the experimental ones have been found already for $U_{\text{eff}} = 3$ eV [30], in the literature there is no consensus about the optional value of U_{eff} (or the values of U and J [28]). Nevertheless, considering the results presented in Fig. 3 and the range of the experimentally determined values of the band gap [47-49], we chose to use $U = 6$ eV hereafter, applied only to the $3d$ states of V. It is also important to observe the impact of the D2 correction on the calculated band gap: PBE+ U +D2 always gives slightly smaller band gaps than PBE+ U . This is the consequence of the decrease of the interlayer spacing (Figs. 1 and 2).

While the effects of the D2 correction and the U term on the lattice parameters are clear, it is also interesting to see how the chemical bonding within a single V_2O_5 layer is affected by them. The calculated bond lengths between vanadium and different oxygen atoms within the V_2O_5 layer (O(1), O(2) and O(3), Fig. 4) are summarized in Table 1.

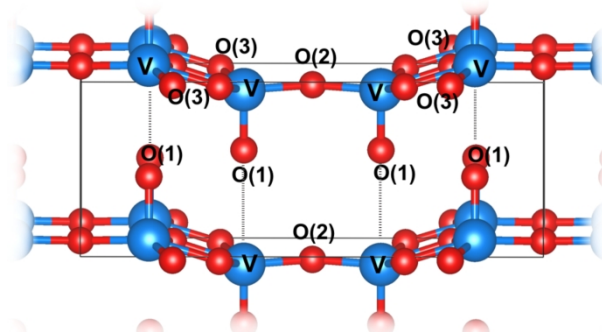


Figure 4. Notation of vanadium and oxygen atoms within a single V_2O_5 layer. Thin dashed lines show the interactions between the vanadyl O atoms of one V_2O_5 layer and vanadium atoms of a subsequent layer which are responsible for layer stacking in the bulk structure.

We note that relative differences between the calculated values and those determined in experiments are only a few percents. There is no single rule about the effect of addition of U or D2 correction on the calculated bond lengths, but, to sum up, we do see that PBE+ U +D2 in principle provides better agreement with experimental data than the PBE+ U scheme (Table 1). We ascribe this to the fact that strong chemical bonding within V_2O_5 layers is only weakly affected by the D2 correction, as discussed also previously for similar systems with strong chemical bonds [51,52]. It appears to be important to describe the interlayer interactions correctly. This is further supported by the fact that the contribution of dispersion interactions *per* V_2O_5 unit in our calculation is around 0.9 eV. This contribution depends only on the configuration of atoms in the simulation cell and it is affected by the value of U in an indirect fashion through the modification of the lattice parameters (Fig. 1). This value closely matches the interlayer binding energies obtained using the vdW-DF methods [34].

Table 1. Calculated vanadium-oxygen bond lengths (in Å) for different computational schemes, compared with the experimental data.

	Bond lengths / Å		
	V–O(1)*	V–O(2)	V–O(3)
PBE	1.580	1.793	2.030/1.892
PBE+D2	1.585	1.786	2.050/1.879
PBE+ U	1.576	1.804	1.982/1.924
PBE+ U +D2	1.579	1.794	1.999/1.908
Experiment*	1.57(5)	1.75(5)	2.03(8)/1.84(7)

*ref. [53]

Analyzing the computational cost of PBE+ U +D2 calculations it can be concluded that the addition of U increases the computational time by approx. 30-40%, whereas the addition of the D2 correction has no noticeable impact on the computational cost. In overall, we conclude that the drawbacks of the GGA approximation in the case of V_2O_5 are successfully compensated for using the combination of DFT+ U and D2 methods. Hence, a relatively small increase of the computational costs for applying PBE+ U +D2 is justified by the obtained results. We further apply the PBE+ U +D2 scheme to study the structural and electronic changes in V_2O_5 upon doping with 3d metals.

3.2. Doped V_2O_5

Having achieved the satisfactory description of the pristine system, we further study how the crystal and electronic structure of bulk V_2O_5 can be modified by doping with 3d metals (from Sc to Zn). As mentioned earlier, we applied the PBE+ U +D2 scheme for all the cases and applied on-site U correction only to the 3d states of vanadium. As we are interested in the overall trends here we chose not to apply U to the d -states of dopants. For comparison, all the calculations were also repeated using PBE, PBE+ U and PBE+D2. We do not present the detailed results of those calculations here but their comparison allows us to conclude that the overall trends are reproduced by all of the approaches. The dopants were introduced either between the V_2O_5 layers or as a substitutional impurity in the layer (Fig. 5).

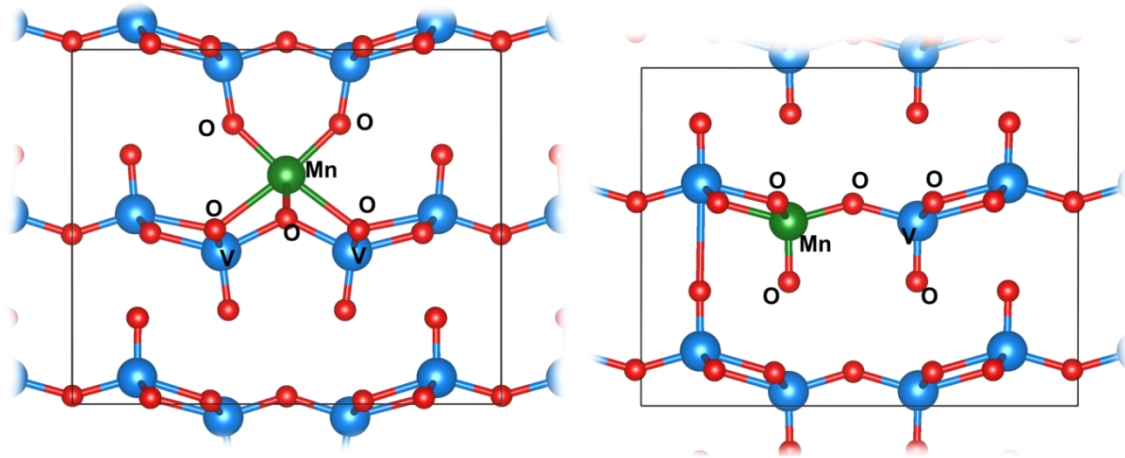


Figure 5. Unit cell of Mn doped V_2O_5 . On the left the case of interstitial doping is shown while on the right substitutional doping is presented.

The volume changes and magnetization induced upon V_2O_5 doping, are presented in Table 2. As can be seen, interstitial doping induces an expansion of the unit cell, which is expected as

the dopant atom is inserted between the V_2O_5 layers. The distance between the two layers accommodating the interstitial dopant increases as compared to the interlayer spacing without the dopant atom in the same system (Fig. 5). The effect of the interstitial impurity is seen for both layers either due to the insertion (pillaring) or due to the impact on the interactions between vanadyl oxygen atoms (O(1) atoms) and the V atoms of the subsequent layer (Fig. 4). In contrast, the unit cell volume of substitutionally doped V_2O_5 is only slightly affected, changing within $\pm 1\%$. In general, the small volume changes obtained for doped V_2O_5 agree with the experimental findings where the orthorhombic structure of parental V_2O_5 is usually found to be preserved. For example, for Cu-doped V_2O_5 only the volume increase by 1.96% was reported but no change of the crystal structure [24]. It should be noted that in the case of doped V_2O_5 the addition of U and D2 corrections has a similar effect as in the case of pristine V_2O_5 . Namely, when the supercell volumes for the PBE and PBE+ U calculations are compared (not presented here), one can see that the latter are larger by roughly 5%. In contrast, when the D2 correction is added to PBE the supercell volume shrinks by approx. 10% for all the cases as a result of enhanced interlayer binding. The same also holds when the D2 correction is added to PBE+ U .

Table 2. Change of the unit cell volume and total magnetization (*per* simulation cell) of doped V_2O_5 obtained by PBE+ U +D2 calculations.

Dopant	$\Delta V^* / \%$		M / μ_B	
	substitutional	interstitial	substitutional	interstitial
Sc	0.81	5.25	2.00	1.00
Ti	-0.75	3.74	1.00	2.00
Cr	-0.25	3.52	1.00	6.00
Mn	-0.60	3.48	2.00	5.00
Fe	-0.31	3.91	3.00	4.00
Co	-0.65	5.01	2.00	3.00
Ni	0.18	1.81	3.00	0.00
Cu	0.61	3.88	2.67	1.00
Zn	0.23	5.89	1.00	1.03

*evaluated as $100 \times (V_{\text{doped}} - V_{\text{pristine}}) / V_{\text{pristine}}$; the volume of pristine $1 \times 1 \times 2$ V_2O_5 supercell is 372.7 \AA^3 using PBE+ U +D2

In addition, an overall net magnetization arises upon the introduction of dopants into the V_2O_5 structure, and its value depends on the dopant type and the way the dopant is introduced into the lattice of V_2O_5 (substitutional/interstitial) (Table 2). In search for the origin of the

magnetization we investigated the spin polarization densities (obtained as $\rho_{\text{spin up}} - \rho_{\text{spin down}}$) and found them to be located at the impurity atoms as well as on the surrounding V and O atoms. The spin polarization densities are presented in Fig. 6 for the case of Fe-doped V_2O_5 . We note that the magnetization is found to be very sensitive to parameter U , and less sensitive to the D2 correction (as seen from the analogous PBE, PBE+ U and PBE+D2 calculations for all the systems). However, all these approaches agree with each other on the appearance of magnetization upon doping of V_2O_5 with 3d elements.

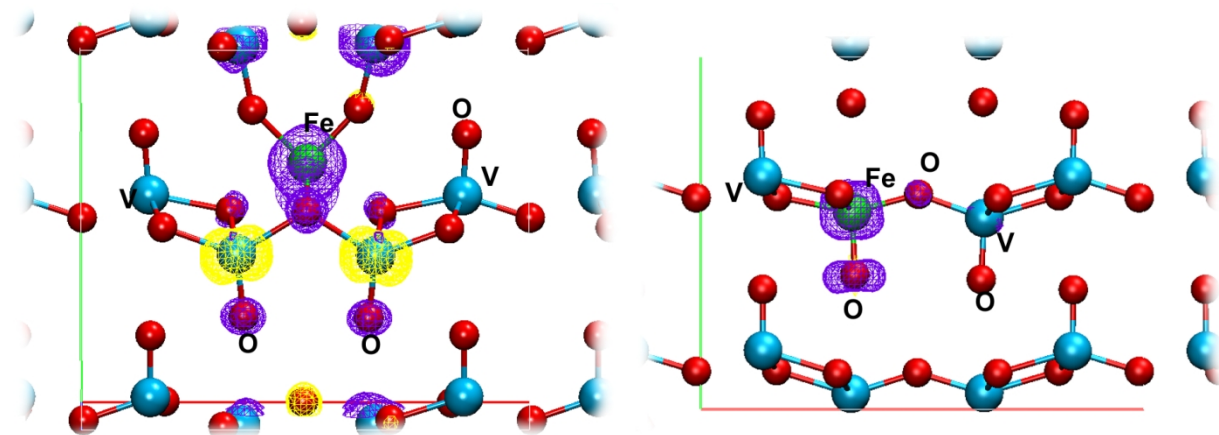


Figure 6. Distribution of spin polarization ($\rho_{\text{spin up}} - \rho_{\text{spin down}}$) for interstitially (left) and substitutionally (right) Fe-doped V_2O_5 (isovalues are $\pm 0.0015 \text{ e } \text{\AA}^{-3}$, positive isosurfaces are marked in purple color, while negative are yellow).

When it comes to the electrochemical applications of materials, conductivity plays a very important role as a hindered electron transport could limit the electrode performance. We investigated the electronic structures of doped V_2O_5 and found that, in general, the band gap becomes narrower due to the introduction of new dopant states (Fig. 7). This indicates that the conductivity of doped V_2O_5 should increase compared to parental V_2O_5 as it was indeed observed in some experimental reports [16–21]. In fact, by inspecting DOSes (Fig. 7) one might see that practically a metallic behavior of otherwise insulating V_2O_5 is expected when doped with the elements between Mn and Ni. Therefore, it is clear that doping can be a powerful strategy for modifying the electrochemical and ion intercalation properties of V_2O_5 . The conclusions derived from the analysis of DOS obtained using PBE+ U +D2 hold also for the results obtained with PBE, PBE+ U and PBE+D2 calculations (not presented here for brevity).

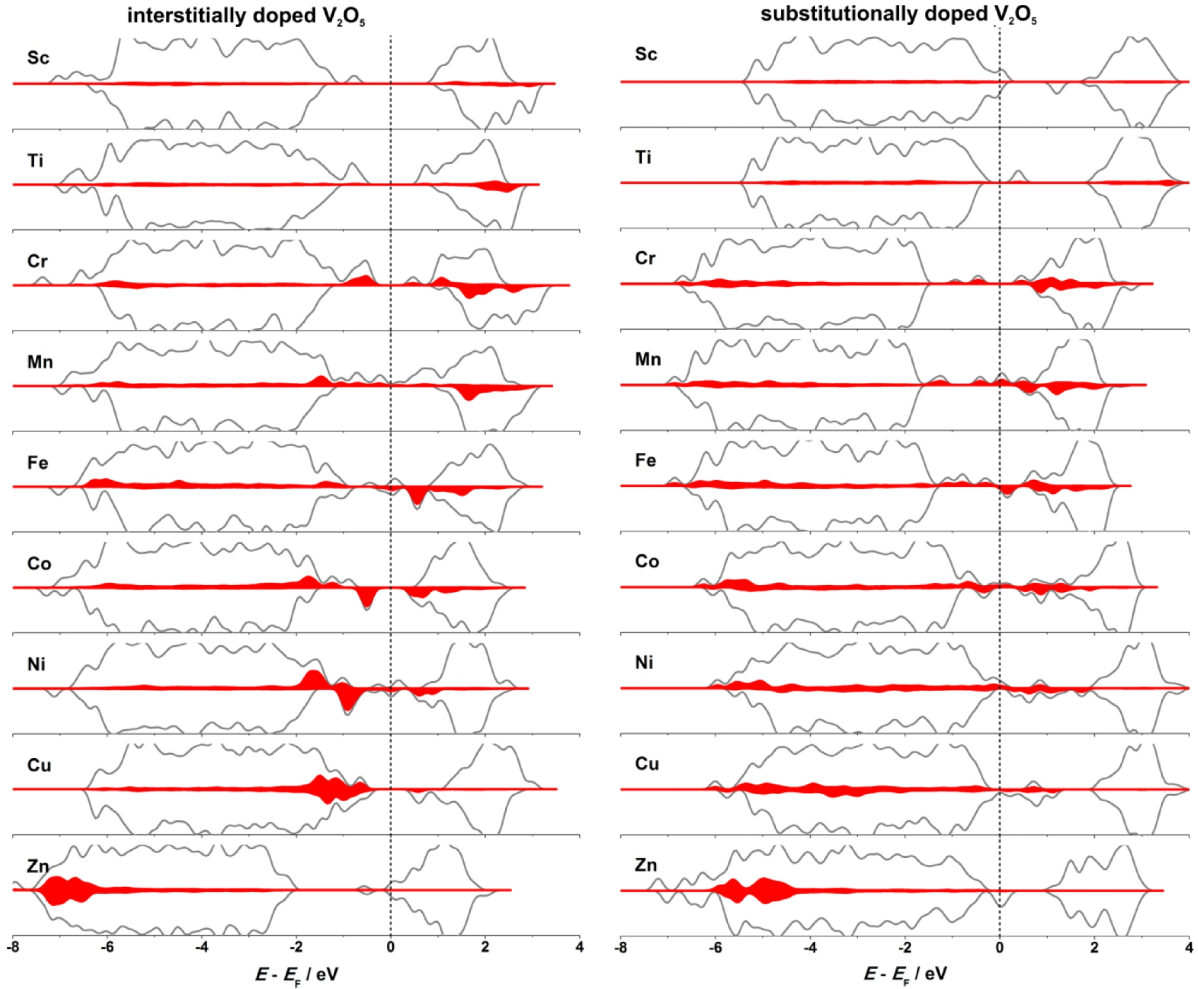


Figure 7. PBE+ U +D2 calculated DOS of interstitially (left) and substitutionally (right) doped V_2O_5 . Projected densities of d -states of dopant atoms (shaded) are also included.

In order to clearly identify the states that appear in the band gap of V_2O_5 upon doping, we analyzed the integrated local density of states (ILDOS, Fig. 8 for the case of Mn-, Fe-, Co- and Ni-doped V_2O_5). We focused on the mentioned dopants causing nearly metallic behavior of doped V_2O_5 . As expected from the DOS plots, the states located in the band gap of V_2O_5 are due to the dopant states and also the states of surrounding V and O atoms (Fig. 8).

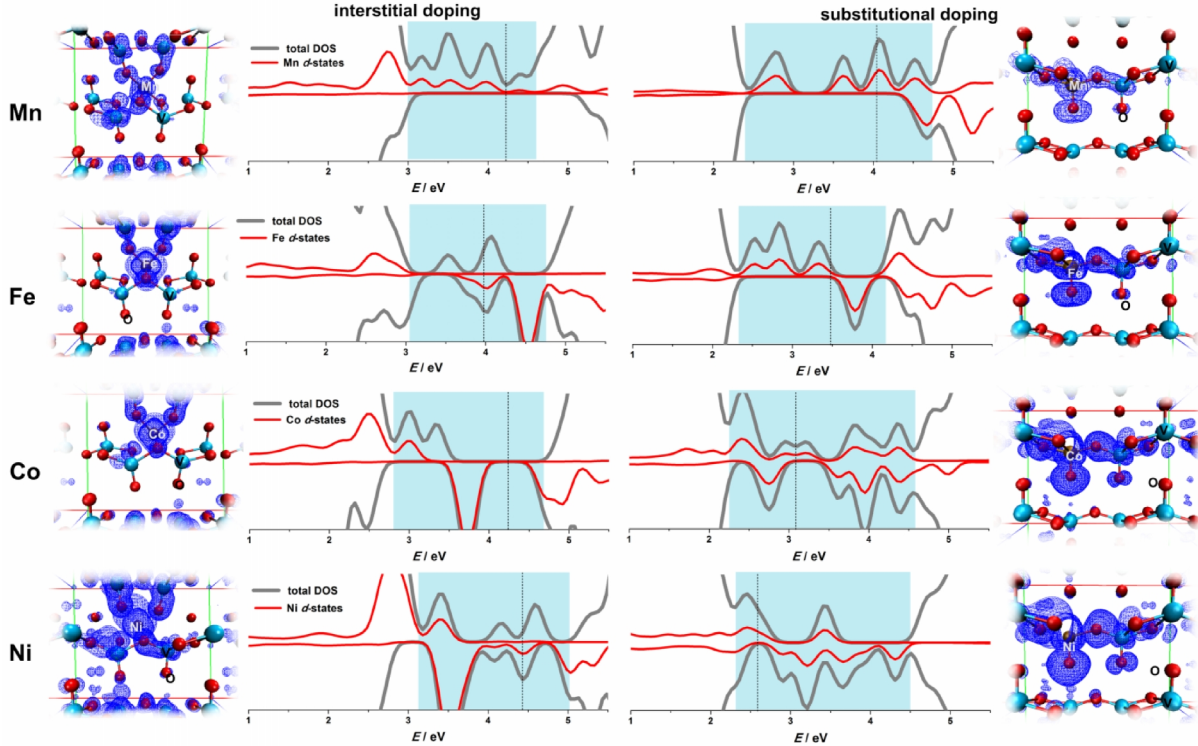


Figure 8. Projected density of states and the corresponding 3D ILDOS maps of the states within the shaded energy window in the DOS plot. The results are presented for the case of V_2O_5 doping with Mn, Fe, Co and Ni (left side – interstitial doping, right side – substitutional doping, isosurfaces value is $0.002 \text{ e} \text{ \AA}^{-3}$). Vertical dashed lines in the DOS plots indicate the Fermi levels.

These states are not highly localized and can indeed contribute to the conductivity of doped V_2O_5 . It is difficult to derive some definite conclusions regarding the specific effects of interstitial vs. substitutional doping. For example, interstitially Co-doped V_2O_5 has a small band gap ($\sim 0.5 \text{ eV}$) while the substitutionally doped one shows a metallic behavior. At the same time Mn-, Fe- and Ni-doped V_2O_5 are metallic, irrespective of the type of doping. However, it is interesting to note that in the case of substitutionally doped V_2O_5 the states located in the band gap span within the layer containing the dopant, while the other layer is like in pristine V_2O_5 , in terms of the electronic structure. On the other hand, in the case of interstitial doping the states are distributed between the layers, which host the impurity. This also indicates that the chemical interactions between the impurities and the V and O atoms of V_2O_5 lattice are more pronounced in the case of substitutional doping and this is also reflected in the overlap between the d -states of the impurity and the valence band of V_2O_5 . For example, one can compare the cases of Co-, Ni- and Cu-doped V_2O_5 (Fig. 7) where it is clear that the d -states of the substitutional impurities span over the entire valence band of V_2O_5 . In contrast, the d -states of interstitial impurities are

predominantly located at the top of valence band. This also means that the chemical properties of interstitial and substitutional impurities, particularly in terms of the interactions with intercalated ions, will be rather different. Finally, a natural question, with no clear answer, remains – whether dopants will prefer substitutional or interstitial positions. Considering volume changes upon doping (Table 2) it seems that the elements from the first half of the 3d row of Periodic Table are relatively easily incorporated into the V_2O_5 lattice. These elements can be found in many oxidation states (especially Cr, Mn and Co) allowing them to replace V^{5+} . In contrast, the elements with almost completed *d*-shell (Ni, Cu, Zn) have a limited number of oxidation states. Hence, we expect that, in reality, it would be difficult for these atoms to adapt to the coordination of V^{5+} in V_2O_5 structure. Naturally, we expect that the preference between substitutional and interstitial doping will also depend on the concentration of dopants. For example, Guan *et al.* [22] described preparation and electrochemical properties of Mn-doped V_2O_5 in a very wide range of concentrations, from $Mn_{0.27}V_2O_5$ (which is very close to our model) to $Mn_{0.94}V_2O_5$. For low Mn concentrations the XRD patterns of Mn-doped V_2O_5 corresponded to that of pure V_2O_5 while for high concentrations of Mn the V_2O_5 interlayer spacing was found to significantly increase. When this result was combined with different types of V=O bonds evidenced in Raman spectra, it was concluded that Mn was inserted between V_2O_5 layers and distorted the V_2O_5 structure. Such different V=O bonds are clearly seen in Fig. 5 for the case of interstitially Mn-doped V_2O_5 . The authors concluded that the structural changes of V_2O_5 , being the consequence of doping, provided more free space for the Li^+ intercalation/de-intercalation. Unfortunately, the same report contains no information about the conductivity of doped V_2O_5 .

4. Conclusions

By employing the combination of the DFT+*U* approach with the semi-empirical DFT+D2 correction for the long-range dispersion interactions, both the crystal and the electronic structure of V_2O_5 were adequately described using periodic plane wave DFT calculations. The inclusion of the D2 correction is of primary importance to address the interlayer spacing in bulk V_2O_5 while the intralayer chemical bonding is not significantly affected by the addition of the *U* term and D2 correction. Within the PBE+*U*+D2 scheme computational costs are increased by roughly 30-40%, which is solely ascribed to the calculation of the *U* term. Using the same approach, we investigated the effects of doping of V_2O_5 by 3d elements, both interstitially and substitutionally. Interstitial doping was found to result in an expansion of the V_2O_5 lattice, while substitutional doping has a much less pronounced effect on the structure of parental V_2O_5 . However, doping induces significant changes of the electronic structure and leads to a narrowing of the band gap

of V_2O_5 . This is expected to result in somewhat higher conductivity of doped V_2O_5 , which was indeed observed in some of the previously published experimental studies. The obtained results suggest that doping can be an elegant strategy for modifying structural and electronic properties of V_2O_5 . This is of crucial importance for the application of this material in the field of metal-ion batteries.

Acknowledgement

This work was supported by the Serbian Ministry of Education, Science, and Technological Development (III45014). S.V.M is indebted to Serbian Academy of Sciences and arts for funding this study through the project “Electrocatalysis in the contemporary processes of energy conversion”. N.V.S. acknowledges the support provided by Swedish Research Council through the project No. 2014-5993. This work was additionally supported by the COMET program by the Austrian Research Promotion Agency (FFG) and the governments of Lower and Upper Austria. We also acknowledge the support from Carl Tryggers Foundation for Scientific Research. The computations were performed on resources provided by the Swedish National Infrastructure for Computing (SNIC) at the High Performance Computing Center North (HPC2N) at Umeå University.

References

- [1] K. Kang, Y.S. Meng, J. Bréger, C.P. Grey, G. Ceder, Electrodes with high power and high capacity for rechargeable lithium batteries., *Science*. 311 (2006) 977–80. doi:10.1126/science.1122152.
- [2] B. Scrosati, J. Hassoun, Y.-K. Sun, Lithium-ion batteries. A look into the future, *Energy Environ. Sci.* 4 (2011) 3287. doi:10.1039/c1ee01388b.
- [3] J. Yao, Y. Li, R.C. Massé, E. Uchaker, G. Cao, Revitalized interest in vanadium pentoxide as cathode material for lithium-ion batteries and beyond, *Energy Storage Mater.* 11 (2018) 205–259. doi:10.1016/j.ensm.2017.10.014.
- [4] Y.M. Zhang, S.X. Bao, T. Liu, T.J. Chen, J. Huang, The technology of extracting vanadium from stone coal in China: History, current status and future prospects, *Hydrometallurgy*. 109 (2011) 116–124. doi:10.1016/j.hydromet.2011.06.002.
- [5] M.S. Whittingham, Lithium batteries and cathode materials, *Chem. Rev.* 104 (2004) 4271–4301. doi:10.1021/cr020731c.
- [6] Y. Wang, K. Takahashi, K. Lee, G. Cao, Nanostructured vanadium oxide electrodes for enhanced lithium-ion intercalation, *Adv. Funct. Mater.* 16 (2006) 1133–1144. doi:10.1002/adfm.200500662.

- [7] J. Livage, Hydrothermal synthesis of nanostructured vanadium oxides, *Materials (Basel)*. 3 (2010) 4175–4195. doi:10.3390/ma3084175.
- [8] I. Stojković, N. Cvjetičanin, S. Marković, M. Mitrić, S. Mentus, Electrochemical Behaviour of V₂O₅ Xerogel and V₂O₅ Xerogel/C Composite in an Aqueous LiNO₃ and Mg(NO₃)₂ Solutions, *Acta Phys. Pol. A*. 117 (2010) 837–840. doi:10.12693/APhysPolA.117.837.
- [9] S.H. Lee, R.A. DiLeo, A.C. Marschilok, K.J. Takeuchi, E.S. Takeuchi, Sol Gel Based Synthesis and Electrochemistry of Magnesium Vanadium Oxide: A Promising Cathode Material for Secondary Magnesium Ion Batteries, *ECS Electrochem. Lett.* 3 (2014) A87–A90. doi:10.1149/2.0021408eel.
- [10] M. Vujković, I. Pašti, I.S. Simatović, B. Šljukić, M. Milenković, S. Mentus, THE INFLUENCE OF INTERCALATED IONS ON CYCLIC STABILITY OF V₂O₅/GRAPHITE COMPOSITE IN AQUEOUS ELECTROLYTIC SOLUTIONS: EXPERIMENTAL AND THEORETICAL APPROACH, *Electrochim. Acta*. 176 (2015) 130–140. doi:10.1016/J.ELECTACTA.2015.07.004.
- [11] R.C. Massé, E. Uchaker, G. Cao, Beyond Li-ion: electrode materials for sodium- and magnesium-ion batteries, *Sci. China Mater.* 58 (2015) 715–766. doi:10.1007/s40843-015-0084-8.
- [12] C. Delmas, H. Cognac-Auradou, J.M. Cocciantelli, M. Ménétrier, J.P. Doumerc, The Li_xV₂O₅ system: An overview of the structure modifications induced by the lithium intercalation, *Solid State Ionics*. 69 (1994) 257–264. doi:10.1016/0167-2738(94)90414-6.
- [13] B.B. Owens, S. Passerini, W.H. Smyrl, Lithium ion insertion in porous metal oxides, *Electrochim. Acta*. 45 (1999) 215–224. doi:10.1016/S0013-4686(99)00205-4.
- [14] Y. Wei, C.W. Ryu, K.B. Kim, Cu-doped V₂O₅ as a high-energy density cathode material for rechargeable lithium batteries, *J. Alloys Compd.* 459 (2008). doi:10.1016/j.jallcom.2007.04.275.
- [15] D. Liu, S. Zhan, G. Chen, W. Pan, C. Wang, Y. Wei, High energy density lithium ion batteries using Li_{2.6}Co_{0.4} - xCu_xN (anode) and Cu_{0.04}V₂O₅ (cathode) electrode materials, *Mater. Lett.* 62 (2008) 4210–4212. doi:10.1016/j.matlet.2008.06.036.
- [16] Y. Wang, K. Lee, H. Shang, B. Wiley, Y. Xia, G. Cao, Ag-Ag_{0.08}V₂O₅ · n H₂O composite films as host materials for Li⁺ intercalation, *Phys. Status Solidi*. 202 (2005) R79–R81. doi:10.1002/pssa.200510026.
- [17] M. Giorgetti, M. Berrettoni, W.H. Smyrl, Doped V₂O₅-Based Cathode Materials: Where Does the Doping Metal Go? An X-ray Absorption Spectroscopy Study, *Chem. Mater.* 19 (2007) 5991–6000. doi:10.1021/cm701910c.
- [18] H.X. Li, L.F. Jiao, H.T. Yuan, M. Zhao, M. Zhang, Y.M. Wang, High-performance Cu-doped vanadium oxide (Cu_xV₂O₅) prepared by rapid precipitation method for rechargeable batteries, *Mater. Lett.* 61 (2007) 101–104.

doi:10.1016/J.MATLET.2006.04.015.

- [19] Y.J. Kim, K.J. Takeuchi, A.C. Marschilok, E.S. Takeuchi, Ag₃V₂P₁₀O₃₂: A High Voltage Silver Vanadium Phosphate Cathode Material, *J. Electrochem. Soc.* 160 (2013) A2207–A2211. doi:10.1149/2.082311jes.
- [20] J.M. Lee, H.-S. Hwang, W.-I. Cho, B.-W. Cho, K.Y. Kim, Effect of silver co-sputtering on amorphous V₂O₅ thin-films for microbatteries, *J. Power Sources.* 136 (2004) 122–131. doi:10.1016/J.JPOWSOUR.2004.05.051.
- [21] C. Xiong, A.E. Aliev, B. Gnade, K.J. Balkus, Fabrication of Silver Vanadium Oxide and V₂O₅ Nanowires for Electrochromics, *ACS Nano.* 2 (2008) 293–301. doi:10.1021/nn700261c.
- [22] S. Guan, Y. Wei, J. Zhou, J. Zheng, C. Xu, A Method for Preparing Manganese-Doped V₂O₅ Films with Enhanced Cycling Stability, *J. Electrochem. Soc.* 163 (2016) H541–H545. doi:10.1149/2.0761607jes.
- [23] H. Yu, X. Rui, H. Tan, J. Chen, X. Huang, C. Xu, W. Liu, D.Y.W. Yu, H.H. Hng, H.E. Hoster, Q. Yan, Cu doped V₂O₅ flowers as cathode material for high-performance lithium ion batteries, *Nanoscale.* 5 (2013) 4937. doi:10.1039/c3nr00548h.
- [24] Y. Wei, C.-W. Ryu, K.-B. Kim, Cu-doped V₂O₅ as a high-energy density cathode material for rechargeable lithium batteries, *J. Alloys Compd.* 459 (2008) L13–L17. doi:10.1016/J.JALLCOM.2007.04.275.
- [25] S.-R. Li, S.-Y. Ge, Y. Qiao, Y.-M. Chen, X.-Y. Feng, J.-F. Zhu, C.-H. Chen, Three-dimensional porous Fe_{0.1}V₂O_{5.15} thin film as a cathode material for lithium ion batteries, *Electrochim. Acta.* 64 (2012) 81–86. doi:10.1016/J.ELECTACTA.2011.12.131.
- [26] S.Y. Zhan, C.Z. Wang, K. Nikolowski, H. Ehrenberg, G. Chen, Y.J. Wei, Electrochemical properties of Cr doped V₂O₅ between 3.8 V and 2.0 V, *Solid State Ionics.* 180 (2009) 1198–1203. doi:10.1016/J.SSI.2009.05.020.
- [27] D.C. Langreth, M. Dion, H. Rydberg, E. Schröder, P. Hyldgaard, B.I. Lundqvist, Van der Waals density functional theory with applications, *Int. J. Quantum Chem.* 101 (2005) 599–610. doi:10.1002/qua.20315.
- [28] A.I. Liechtenstein, V.I. Anisimov, J. Zaanen, Density-functional theory and strong interactions: Orbital ordering in Mott-Hubbard insulators, *Phys. Rev. B.* 52 (1995) R5467–R5470. doi:10.1103/PhysRevB.52.R5467.
- [29] S.L. Dudarev, G.A. Botton, S.Y. Savrasov, C.J. Humphreys, A.P. Sutton, Electron-energy-loss spectra and the structural stability of nickel oxide: An LSDA+U study, *Phys. Rev. B.* 57 (1998) 1505–1509. doi:10.1103/PhysRevB.57.1505.
- [30] V.A. Ranea, P.L.D. Quiña, The structure of the bulk and the (001) surface of V₂O₅. A DFT+U study, *Mater. Res. Express.* 3 (2016) 85005. doi:10.1088/2053-1591/3/8/085005.

- [31] R.-P. Blum, H. Niehus, C. Hucho, R. Fortrie, M. V. Ganduglia-Pirovano, J. Sauer, S. Shaikhutdinov, H.-J. Freund, Surface Metal-Insulator Transition on a Vanadium Pentoxide (001) Single Crystal, *Phys. Rev. Lett.* 99 (2007) 226103. doi:10.1103/PhysRevLett.99.226103.
- [32] T. Kerber, M. Sierka, J. Sauer, Application of semiempirical long-range dispersion corrections to periodic systems in density functional theory, *J. Comput. Chem.* 29 (2008) 2088–2097. doi:10.1002/jcc.21069.
- [33] E. Londero, E. Schröder, Vanadium pentoxide (V₂O₅): A van der Waals density functional study, *Comput. Phys. Commun.* 182 (2011) 1805–1809. doi:10.1016/J.CPC.2010.12.036.
- [34] E. Londero, E. Schröder, Role of van der Waals bonding in the layered oxide V₂O₅: First-principles density-functional calculations, *Phys. Rev. B.* 82 (2010) 54116. doi:10.1103/PhysRevB.82.054116.
- [35] M. Dion, H. Rydberg, E. Schröder, D.C. Langreth, B.I. Lundqvist, Van der Waals Density Functional for General Geometries, *Phys. Rev. Lett.* 92 (2004) 246401. doi:10.1103/PhysRevLett.92.246401.
- [36] M. Dion, H. Rydberg, E. Schröder, D.C. Langreth, B.I. Lundqvist, Erratum: Van der Waals Density Functional for General Geometries [*Phys. Rev. Lett.* 92, 246401 (2004)], *Phys. Rev. Lett.* 95 (2005) 109902. doi:10.1103/PhysRevLett.95.109902.
- [37] K. Lee, É.D. Murray, L. Kong, B.I. Lundqvist, D.C. Langreth, Higher-accuracy van der Waals density functional, *Phys. Rev. B.* 82 (2010) 81101. doi:10.1103/PhysRevB.82.081101.
- [38] S. Grimme, Semiempirical GGA-type density functional constructed with a long-range dispersion correction, *J. Comput. Chem.* 27 (2006) 1787–1799. doi:10.1002/jcc.20495.
- [39] J.P. Perdew, K. Burke, M. Ernzerhof, D. of Physics, N.O.L. 70118 J. Quantum Theory Group Tulane University, Generalized Gradient Approximation Made Simple, *Phys. Rev. Lett.* 77 (1996) 3865–3868. doi:10.1103/PhysRevLett.77.3865.
- [40] P. Giannozzi, S. Baroni, N. Bonini, M. Calandra, R. Car, C. Cavazzoni, D. Ceresoli, G.L. Chiarotti, M. Cococcioni, I. Dabo, A. Dal Corso, S. de Gironcoli, S. Fabris, G. Fratesi, R. Gebauer, U. Gerstmann, C. Gougoussis, A. Kokalj, M. Lazzeri, L. Martin-Samos, N. Marzari, F. Mauri, R. Mazzarello, S. Paolini, A. Pasquarello, L. Paulatto, C. Sbraccia, S. Scandolo, G. Sclauzero, A.P. Seitsonen, A. Smogunov, P. Umari, R.M. Wentzcovitch, QUANTUM ESPRESSO: a modular and open-source software project for quantum simulations of materials., *J. Phys. Condens. Matter.* 21 (2009) 395502. doi:10.1088/0953-8984/21/39/395502.
- [41] D. Vanderbilt, Soft self-consistent pseudopotentials in a generalized eigenvalue formalism, *Phys. Rev. B.* 41 (1990) 7892–7895. doi:10.1103/PhysRevB.41.7892.

- [42] M. Cococcioni, S. de Gironcoli, Linear response approach to the calculation of the effective interaction parameters in the LDA + U method, *Phys. Rev. B.* 71 (2005) 35105. doi:10.1103/PhysRevB.71.035105.
- [43] W. Humphrey, A. Dalke, K. Schulten, VMD: Visual molecular dynamics, *J. Mol. Graph.* 14 (1996) 33–38. doi:10.1016/0263-7855(96)00018-5.
- [44] K. Momma, F. Izumi, IUCr, *VESTA*: a three-dimensional visualization system for electronic and structural analysis, *J. Appl. Crystallogr.* 41 (2008) 653–658. doi:10.1107/S0021889808012016.
- [45] M. V. Ganduglia-Pirovano, J. Sauer, Stability of reduced V₂O₅ (001) surfaces, *Phys. Rev. B.* 70 (2004) 45422. doi:10.1103/PhysRevB.70.045422.
- [46] D.M. Carrillo-Flores, M.T. Ochoa-Lara, F. Espinosa-Magaña, Electron energy-loss spectroscopy of V₂O₅ nanofibers synthesized by electro-spinning, *Micron.* 52–53 (2013) 39–44. doi:10.1016/J.MICRON.2013.07.010.
- [47] R. Zimmermann, P. Steiner, R. Claessen, F. Reinert, S. Hüfner, P. Blaha, P. Dufek, Electronic structure of 3d-transition-metal oxides: on-site Coulomb repulsion versus covalency, *J. Phys. Condens. Matter.* 11 (1999) 1657–1682. doi:10.1088/0953-8984/11/7/002.
- [48] E.E. Chain, Optical properties of vanadium dioxide and vanadium pentoxide thin films, *Appl. Opt.* 30 (1991) 2782. doi:10.1364/AO.30.002782.
- [49] J. Meyer, K. Zilberberg, T. Riedl, A. Kahn, Electronic structure of Vanadium pentoxide: An efficient hole injector for organic electronic materials, *J. Appl. Phys.* 110 (2011) 33710. doi:10.1063/1.3611392.
- [50] L. Wang, T. Maxisch, G. Ceder, Oxidation energies of transition metal oxides within the GGA + U framework, *Phys. Rev. B.* 73 (2006) 195107. doi:10.1103/PhysRevB.73.195107.
- [51] J.O. Nilsson, M. Leetmaa, B. Wang, P.A. Žgunc, I. Pašti, A. Sandell, N. V. Skorodumova, Modeling Kinetics of Water Adsorption on the Rutile TiO₂ (110) Surface: Influence of Exchange-Correlation Functional, *Phys. Status Solidi.* (2017) 1700344. doi:10.1002/pssb.201700344.
- [52] A.S. Dobrota, I.A. Pašti, S. V. Mentus, B. Johansson, N. V. Skorodumova, Functionalized graphene for sodium battery applications: the DFT insights, *Electrochim. Acta.* 250 (2017) 185–195. doi:10.1016/J.ELECTACTA.2017.07.186.
- [53] R. Enjalbert, J. Galy, IUCr, A refinement of the structure of V₂O₅, *Acta Crystallogr. Sect. C Cryst. Struct. Commun.* 42 (1986) 1467–1469. doi:10.1107/S0108270186091825.